Vol 4 (2) (2023)

Measurement, Control, and Automation

Website: https:// mca-journal.org

ISSN 1859-0551

Predictive Direct Power Control of Grid-Connected PV Systems

Son T. Nguyen[1]*, Tu M. Pham[1], Anh Hoang[1], Tuan V. Pham[2]

[1]Hanoi University of Science and Technology, Vietnam
[2]Vinh University of Technology Education, Vietnam
[*]Corresponding author E-mail: son.nguyenthanh@hust.edu.vn

Abstract

This paper presents an effective grid-injected power control method for a photovoltaic (PV) system using the theory of model predictive control (MPC). The system consists of two power converters including a DC/DC boost converter for maximum point point tracking (MPPT) and a DC/AC converter formed by a two-level voltage-source three-phase inverter. Future values of the grid-injected active and reactive power can be predicted by using the inverter model and the discrete-time model of the load. A cost function is defined based on the differences of the reference and predictive power. The optimal switching state of the inverter at each sampling period is selected corresponding to the minimum value of the cost function. In addition, the desired grid-injected active and reactive power can be obtained by simply setting the reference active and reactive power in the cost function. The main advantage of this control method is that it does not require the use of any external current controller and pulse width modulation (PWM) techniques such as sinusoidal pulse width modulation (SPWM) or space vector pulse width modulation (SVPWM). Moreover, the predictive direct power control does not use a phase locked loop (PLL) usually required for the conventional current control methods of the grid-connected inverter. The simulation results obtained using MATLAB/Simulink verify the effectiveness of the proposed method.

***Keywords**: Grid-connected PV systems, direct power control, model predictive control*

Abbreviations

PV	Photovoltaic
MPC	Model predictive control
PDPC	Predictive direct power control
ANN	Artificial neural network
FL	Fuzzy logic
MPPT	Maximum power point tracking
P&O	Perturb and Observe
DC	Direct current
AC	Alternating current
SPWM	Sinusoidal pulse with modulation
SVPWM	Space vector pulse width modulation
PLL	Phase locked loop

Tóm tắt

Bài báo này trình bày một phương pháp điều khiển hiệu quả công suất của một hệ thống quang điện nối lưới sử dụng lý thuyết điều khiển dự báo mô hình. Hệ thống bao gồm một bộ biến đổi DC/DC để bám điểm công suất cực đại (MPPT) và một bộ biến đổi DC/AC sử dụng một bộ nghịch lưu ba pha nguồn áp hai mức. Các giá trị tương lai của công suất tác dụng và công suất phản kháng phát vào lưới có thể được dự báo bằng cách sử dụng mô hình của bộ nghịch lưu và mô hình thời gian rời rạc của tải. Một hàm chi phí được định nghĩa dựa trên sai khác giữa công suất tham chiếu và công suất dự báo. Trạng thái chuyển mạch tối ưu của bộ nghịch lưu được xác định ứng với giá trị nhỏ nhất của hàm chi phí trong mỗi chu kỳ lấy mẫu. Thêm vào đó công suất tác dụng và công suất biểu kiến phát vào lưới có thể đạt được bằng cách đơn giản đặt giá trị tham chiếu cho công suất tác dụng và công suất phản kháng trong hàm chi phí.
Ưu điểm chính của phương pháp điều khiển này là không yêu cầu sử dụng bất kỳ một bộ điều khiển dòng điện vòng ngoài hay các bộ điều biến độ rộng xung như điều biến độ rộng xung sin (SPWM) hay điều biến độ rộng xung véc tơ không gian (SVPWM). Hơn thế nữa, điều khiển công suất dự báo trực tiếp không đòi hỏi việc sử dụng vòng khóa pha (PLL) như các phương pháp điều khiển dòng điện truyền thống cho các bộ nghịch lưu nối lưới. Kết quả mô phỏng thu được bằng MATLAB/Simulink khẳng định tính hiệu quả của phương pháp đề xuất.

1. Introduction

The lack of fossil energy and the increase of air pollution have resulted in the wide use of various renewable energy sources. Due to the low prices of PV panels, PV systems have been used as the most popular renewable energy source. The output voltage of a PV module is usually lower than the peak value of the grid voltage and varies in a wide range according to its different operation conditions. Therefore, series and parallel connections of PV panels to form a PV array can be seen as a simple way to increase the output voltage [1].
To obtain a higher output voltage from a PV array, a DC/DC boost converter is often used. This converter can be controlled to derive the maximum output power from the PV array. In various MPPT techniques for PV systems, the P&O algorithm is widely used due to its effectiveness and ease of implementation [2].

Received: 6 January 2023; Accepted: 18 May 2023.

In a grid-connected PV system, the combination of the PV array and DC/DC boost converter can be seen as a DC source for a DC/AC converter (inverter), which is controlled to inject the desired active and reactive power into the grid [3]. To avoid the negative influences of harmonics components from the currents generated by the inverter on the grid, these currents are usually required to have very low harmonics. As the grid-injected currents are in the phase with the grid voltage, the maximum active power can be obtained [1].

In conventional current control methods of the inverter, a linear current controller for the inverter has been used to maintain stable operation of the system as it can effectively regulate the output current to track the reference current [3], [4]. A sliding-mode current controller for a grid-connected PV system is proposed in [5]. In addition, intelligent techniques based on artificial neural networks (ANNs) and fuzzy logic (FL) are also proposed for the improved control of grid-connected PV systems [6, 7]. These control methods of two-level voltage-source three-phase inverters often require the use of SPMW and SVPWM.

Recently, the MPC theory has been applied to advanced controls of power converters [8, 9]. In this control approach, a discrete model of the system is used to predict the future behaviors of variables over a time frame. Next, these variable predictions are utilized to minimize a cost function for optimally choosing a sequence of the control action.

In this paper, a predictive direct power control (PDPC) algorithm for the grid-injected active and reactive power control of a PV system is described in detail. The remainder of this paper is organized into the following sections: In Section 2, a PV system is briefly described. Section 3 presents the model of the grid-connected two-level voltage-source three-phase inverter and discrete-time model of the three-phase load. In Section 4, the classical current control methods of the grid-connected three-phase inverter is mentioned. MPC of the grid-connected three-phase inverter is described in detail in Section 5. Simulation results and discussions are presented in Section 6. Finally, Section 7 is the conclusion of this research.

2. PV Systems

A PV array is formed by connecting PV panels in series and/or parallel. However, when a load is directly connected to the output of the PV array, the operating point of the PV array is rarely at the point corresponding to the maximum output power. The operating point of the PV array depends on the impedance seen by the PV array. As a result, the operating point of the PV array can be moved towards the peak power point by changing the impedance seen by the PV array.

As the PV array is a DC source, a DC-DC boost converter is usually used for transforming the impedance of the source to the load as shown in Figure 1. The change of the duty cycle of the boost converter results in the variation of the impedance seen by the PV array. At a particular impedance corresponding to a specific duty cycle, the operating point can be at the peak power transfer point.

In maximum power point tracking (MPPT) algorithms, the PV array voltage and current are sampled to appropriately adjust the duty cycle. In P&O method as shown in Figure 2, the voltage from the PV array is slightly adjusted and the power is then measured. If the power increases, additional adjustments in that direction are performed until the power tends not to rise anymore.

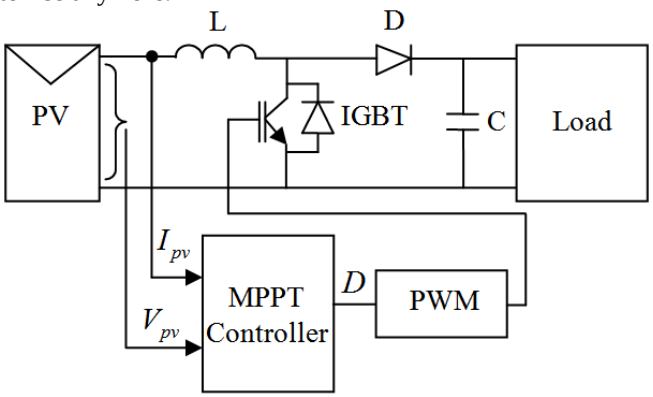

Figure 1: A PV system with MPPT using a DC-DC boost converter.

The relationship between the output and input voltage of the boost converter is given by:

$$V_{out} = \frac{1}{1-D} V_{in} \tag{1}$$

where V_{in} and V_{out} are the input and output voltage, respectively. D is the duty cycle.

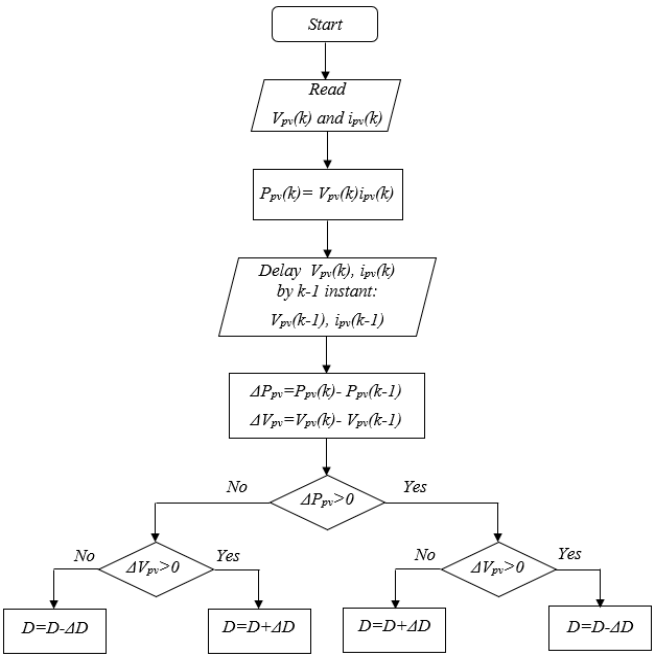

Figure 2: Flowchart of the P&O MPPT method.

3. Model of Grid-Connected Three-Phase Inverter

3.1. Inverter Model

The power circuit of a grid-connected two-level voltage-source three-phase inverter is shown in Figure 3. V_{dc} is the DC link voltage, L is the filtering inductance and R is the

line resistance. e_a is the grid voltage of phase A. i_a is the output current of phase A.

To describe the switching states of the inverter, the variables S_a, S_b and S_c are defined as follows:

- $S_a = 1$ if S_1 on and S_4 off
- $S_a = 0$ if S_1 off and S_4 on
- $S_b = 1$ if S_2 on and S_5 off
- $S_b = 0$ if S_2 off and S_5 on
- $S_c = 1$ if S_3 on and S_6 off
- $S_c = 0$ if S_3 off and S_6 on

These switching signals can be used to define the values of the output voltage as follows:

$$v_{aN} = S_a V_{dc} \tag{2}$$

$$v_{bN} = S_b V_{dc} \tag{3}$$

$$v_{cN} = S_c V_{dc} \tag{4}$$

where v_{aN}, v_{bN} and v_{cN} are the phase-to-neutral voltages of the inverter.

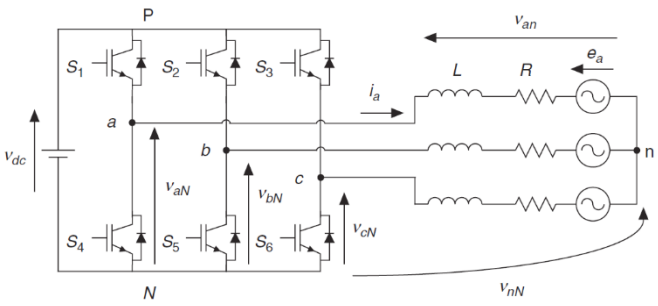

Figure 3: Two-level voltage-source three phase inverter power circuit.

The inverter output voltage vector v is defined as follows:

$$v = \frac{2}{3}\left(v_{aN} + a v_{bN} + a^2 v_{cN}\right) \tag{5}$$

where a is the unitary vector and $a = e^{i2\pi/3} = -\frac{1}{2} + j\frac{\sqrt{3}}{2}$.

Possible combinations of the switching states can generate the voltage vectors, which can be also represented in a complex plane as shown in Figure 4. Table 1 is the switching states and corresponding voltage vectors. However, the voltage vectors generated by the inverter are only seven different vectors as V_0 and V_7 produce the same zero vector ($V_0 = V_7$). This means that a two-level voltage-source three-phase inverter can only generate 7 different voltage vectors.

The output voltage of the inverter is determined as

$$\begin{bmatrix} v_\alpha \\ v_\beta \end{bmatrix} = \frac{2}{3}\begin{bmatrix} 1 & -\frac{1}{2} & -\frac{1}{2} \\ 0 & \frac{\sqrt{3}}{2} & -\frac{\sqrt{3}}{2} \end{bmatrix}\begin{bmatrix} v_{aN} \\ v_{bN} \\ v_{cN} \end{bmatrix} \tag{6}$$

Substituting (2), (3) and (4) into (6) gives

$$v_\alpha = \frac{1}{3}(2S_a - S_b - S_c)V_{dc} \tag{7}$$

$$v_\beta = \frac{2}{3}\left(\frac{\sqrt{3}}{2}S_b - \frac{\sqrt{3}}{2}S_c\right)V_{dc} \tag{8}$$

Table 1: Switching states and voltage vectors.

S_a	S_b	S_c	Voltage vector V
0	0	0	$V_0 = 0$
1	0	0	$V_1 = 2/3V_{dc}$
1	1	0	$V_2 = 1/3V_{dc} + j\sqrt{3}/2V_{dc}$
0	1	0	$V_3 = -1/3V_{dc} + j\sqrt{3}/3V_{dc}$
0	1	1	$V_4 = -2/3V_{dc}$
0	0	1	$V_5 = -1/3V_{dc} - j\sqrt{3}/3V_{dc}$
1	0	1	$V_6 = 1/3V_{dc} - j\sqrt{3}/3V_{dc}$
1	1	1	$V_7 = 0$

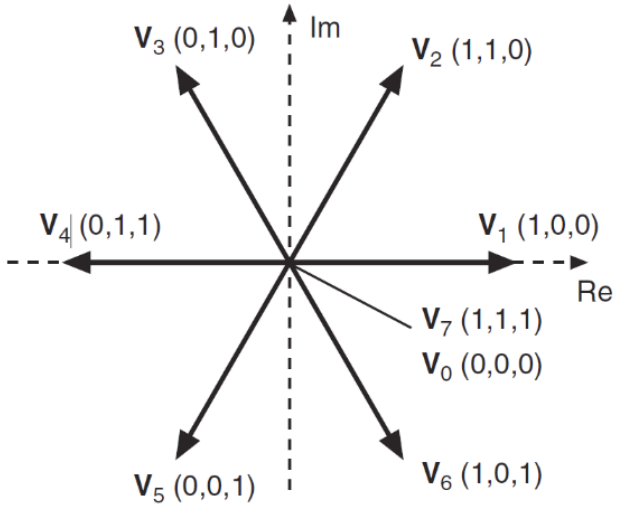

Figure 4: Voltage vectors in the complex plane.

3.2. Load Model

The dynamic equation of the grid-connected current has the following form:

$$v = Ri + L\frac{di}{dt} + e \tag{9}$$

where v is the voltage vector generated by the inverter, i the load current vector and e is the load back-emf vector. In simulations and experiments, e is assumed to be sinusoidal with constant amplitude and constant frequency.

3.3. Discrete-Time Model for Prediction

The Clark transforms from the abc-frame to the $\alpha\beta$-frame applied to the load current vector and the load back-emf vector has the following forms:

$$\begin{bmatrix} i_\alpha \\ i_\beta \end{bmatrix} = \frac{2}{3}\begin{bmatrix} 1 & -\frac{1}{2} & -\frac{1}{2} \\ 0 & \frac{\sqrt{3}}{2} & -\frac{\sqrt{3}}{2} \end{bmatrix}\begin{bmatrix} i_a \\ i_b \\ i_c \end{bmatrix} \quad (10)$$

$$\begin{bmatrix} e_\alpha \\ e_\beta \end{bmatrix} = \frac{2}{3}\begin{bmatrix} 1 & -\frac{1}{2} & -\frac{1}{2} \\ 0 & \frac{\sqrt{3}}{2} & -\frac{\sqrt{3}}{2} \end{bmatrix}\begin{bmatrix} e_a \\ e_b \\ e_c \end{bmatrix} \quad (11)$$

Equation (9) can be expressed in the $\alpha\beta$-frame as follows:

$$\begin{bmatrix} v_\alpha \\ v_\beta \end{bmatrix} = R\begin{bmatrix} i_\alpha \\ i_\beta \end{bmatrix} + L\frac{d}{dt}\begin{bmatrix} i_\alpha \\ i_\beta \end{bmatrix} + \begin{bmatrix} e_\alpha \\ e_\beta \end{bmatrix} \quad (12)$$

If the sampling time is defined as T_s, then the current equations in the $\alpha\beta$-frame in discrete-time can be approximated as follows:

$$\frac{d}{dt}\begin{bmatrix} i_\alpha(k+1) \\ i_\beta(k+1) \end{bmatrix} \approx \frac{1}{T_s}\begin{bmatrix} i_\alpha(k+1)-i_\alpha(k) \\ i_\beta(k+1)-i_\beta(k) \end{bmatrix} \quad (13)$$

The discrete form of equation (13) in the $\alpha\beta$-frame at the $(k+1)$-th sampling period is given by:

$$\begin{bmatrix} v_\alpha(k+1) \\ v_\beta(k+1) \end{bmatrix} = R\begin{bmatrix} i_\alpha(k+1) \\ i_\beta(k+1) \end{bmatrix} + \frac{L}{T_s}\begin{bmatrix} i_\alpha(k+1)-i_\alpha(k) \\ i_\beta(k+1)-i_\beta(k) \end{bmatrix} + \begin{bmatrix} e_\alpha(k+1) \\ e_\beta(k+1) \end{bmatrix} \quad (14)$$

For a sufficient small sampling period with respect to the grid fundamental frequency, it can be assumed that $v_\alpha(k+1) \approx v_\alpha(k)$, $v_\beta(k+1) \approx v_\beta(k)$, $e_\alpha(k+1) \approx e_\alpha(k)$ and $e_\beta(k+1) \approx e_\beta(k)$. Then, equation (14) can be re-written as follows:

$$\begin{bmatrix} v_\alpha(k) \\ v_\beta(k) \end{bmatrix} = R\begin{bmatrix} i_\alpha(k+1) \\ i_\beta(k+1) \end{bmatrix} + \frac{L}{T_s}\begin{bmatrix} i_\alpha(k+1)-i_\alpha(k) \\ i_\beta(k+1)-i_\beta(k) \end{bmatrix} + \begin{bmatrix} e_\alpha(k) \\ e_\beta(k) \end{bmatrix} \quad (15)$$

From equation (15), the predicted currents at the $(k+1)$-th sampling period can be obtained from the currents at the k-th sampling period as follows:

$$\begin{bmatrix} i_\alpha(k+1) \\ i_\beta(k+1) \end{bmatrix} = \left(\frac{T_s}{RT_s+L}\right)\begin{bmatrix} v_\alpha(k)-e_\alpha(k) \\ v_\beta(k)-e_\beta(k) \end{bmatrix} + \left(\frac{L}{RT_s+L}\right)\begin{bmatrix} i_\alpha(k) \\ i_\beta(k) \end{bmatrix} \quad (16)$$

Next, the predicted instantaneous output active and reactive power seen from the grid side at the $(k+1)$-th sampling period can be formed as follows:

$$P_{out}(k+1) = -\frac{3}{2}\left[e_\alpha(k)i_\alpha(k+1) + e_\beta(k)i_\beta(k+1)\right] \quad (17)$$

$$Q_{out}(k+1) = -\frac{3}{2}\left[e_\beta(k)i_\alpha(k+1) - e_\alpha(k)i_\beta(k+1)\right] \quad (18)$$

3.4. Cost Function

A. Cost Function for Current Control

The predictive currents in (16) can be used to define a cost function as follows:

$$g = \left|i_\alpha^*(k) - i_\alpha(k+1)\right| + \left|i_\beta^*(k) - i_\beta(k+1)\right| \quad (19)$$

where $i_\alpha^*(k)$ and $i_\alpha^*(k)$ are the reference currents.

B. Cost Function for Power Control

The predictive active and reactive power in (17) and (18) can be used to define a cost function as follows:

$$g = \left|P_{out}^* - P_{out}(k+1)\right| + \left|Q_{out}^* - Q_{out}(k+1)\right| \quad (20)$$

If the reactive power needs to be minimized, the cost function yields:

$$g = \left|P_{out}^* - P_{out}(k+1)\right| + \left|Q_{out}(k+1)\right| \quad (21)$$

4. Classical Current Control of Grid-Connected Three-Phase Inverter

4.1. Hysteresis Current Control

The basic idea of the hysteresis current control is to keep the current inside the hysteresis band by changing the switching state of the converter each time the current reaches the boundary. For a three-phase inverter, measured load currents of each phase are compared to the corresponding references using hysteresis comparators.

4.2. Sinusoidal PWM Current Control

In sinusoidal PWM (SPWM), a sinusoidal reference voltage is compared to the triangular carrier signal generating a pulsed voltage waveform at the output of the inverter. The fundamental component of this voltage is proportional to the reference voltage.

4.3. Space Vector PWM Current Control

Space vector PWM (SVPWM) can be seen as a variation of PWM techniques, in which the application times of the voltage vectors of the inverter are calculated from the reference vector V_s^* as shown in Figure 5. For sector k ($k = 1,...,6$), V_k and V_{k+1} are the adjacent vectors and V_0 is the zero vector applied during t_k, t_{k+1} and t_0.

$$v_s^* = V_k t_k + V_{k+1} t_{k+1} + V_0 t_0 \tag{22}$$

$$T = t_k + t_{k+1} + t_0 \tag{23}$$

where T is the carrier period and t_k/T, t_{k+1}/T and t_0/T are the duty cycles of their respective vectors.

$$t_k = \frac{3T|v_s^*|}{2V_{dc}}\left(\cos(\theta-\theta_k) - \frac{\sin(\theta-\theta_k)}{\sqrt{3}}\right) \tag{24}$$

$$t_{k+1} = \frac{3T|v_s^*|}{V_{dc}}\frac{\sin(\theta-\theta_k)}{\sqrt{3}} \tag{25}$$

$$t_0 = T - t_k - t_{k+1} \tag{26}$$

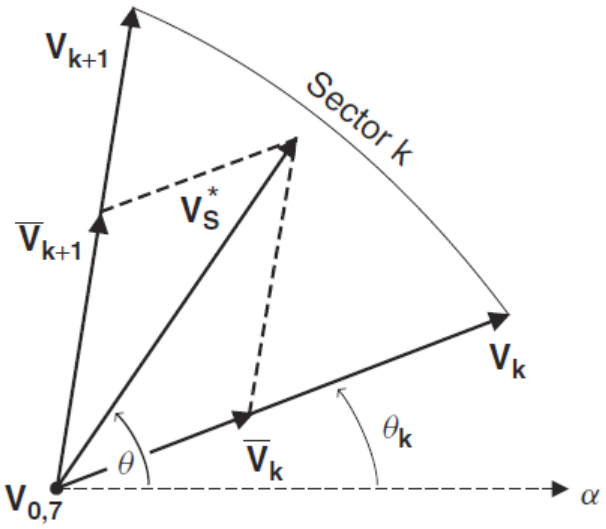

Figure 5: Generation of the reference voltage vector in a generic sector.

5. Model Predictive Control of Grid-Connected Three-Phase Inverter

Figure 6 is the principle of MPC for the three-phase inverter. The control method requires the measurement of the grid current i_g and the grid voltage e_g. The predictive model for the current and power can be formed using equation (16), (17) and (18). In each sampling period, the optimal switching state of the inverter is determined according to the minimum of seven values of the cost function.

The amount of the grid-injected active power is tightly related to the maximum power generated by the DC/DC boost converter. This control action also requires maintaining the DC link voltage at a desired constant value. Therefore, the reference of the active power can be given by using a linear controller such as a proportional-integral (PI) controller for the DC link voltage.

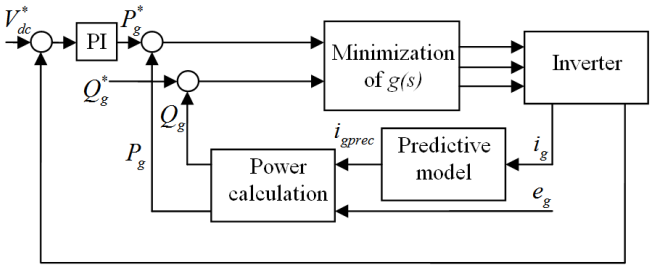

Figure 6: Principle of MPC for three-phase inverter.

6. Simulation Results

6.1. Current Control Methods of Grid-Connected Three-Phase Inverters

In this section, different current control methods of grid-connected three-phase inverters are investigated based on MATLAB/Simulink simulation. These current control methods include:

- Hysteresis current control
- Sinusoidal PWM current control
- Space vector PWM current control
- Predictive direct current control

Table 2 is the parameters of the three-phase inverter used for simulation. Firstly, the reference current is assumed to have the following equation:

$$i_{ref} = 10\sin(\omega t)$$

At the time of 0,1 second, the reference current has the following equation:

$$i_{ref} = 20\sin(\omega t)$$

Table 2: Parameters of the three-phase inverter used for simulation.

Parameters	Values
Reference DC link voltage	Vdc_ref = 800 (V)
Filtering inductance	L = 0.01 (mH)
Line resistance	R = 1 (Ω)
Phase to phase grid voltage	e = 380 (V)

Figure 7 is the Simulink diagram of the hysteresis current control. Figure 8(a) is the current waveforms and Figure 8(b) is the grid-injected active and reactive power. Figure 9(a) is the current waveforms and Figure 9(b) is the FFT of the current. Figure 10 is the Simulink diagram of the SPWM current control. Figure 11(a) is the current waveforms and Figure 11(b) is the grid-injected active and reactive power. Figure 12(a) is the current waveforms and Figure 12(b) is the FFT of the current.

Figure 13 is the Simulink diagram of the SVPWM current control. Figure 14(a) is the current waveforms and Figure 14(b) is the grid-injected active and reactive power. Figure 15(a) is the current waveforms and Figure 15(b) is the FFT of the current.

Figure 16 is the Simulink diagram of the predictive direct current control. Figure 17(a) is the current waveforms and Figure 17(b) is the grid-injected active and reactive power. Figure

18(a) is the current waveforms and Figure 18(b) is the FFT of the current.

Table 3 is total harmonic distortions (THDs) of the currents corresponding to four current control methods. Table 4 shows the techniques required for the current control methods. Obviously, the hysteresis current control and predictive direct current controls do not require the use of any PWM techniques.

For most of the current control methods, a PLL is required to ensure the grid voltage in the phase with the grid current. Then, the maximum of the grid-injected active power can be obtained. However, the predictive direct power control method does not need a PLL.

Table 3: Total harmonic distortion (THD (%)) of the phase current.

Current control method	Phase A	Phase B	Phase C
Hysteresis current control	1.314	1.353	1.348
SPWM current control	8.534	8.54	8.583
SVPWM current control	2.592	2.573	2.672
Predictive direct current control	0.943	1.053	1.059

Table 4: The techniques required to develop the control algorithms.

Current control method	Transformation	PWM
Hysteresis current control	dq0/abc	No
SPWM current control	abc/dq0; dq0/abc	Yes
SVPWM current control	abc/dq0; dq0/abc	Yes
Predictive direct current control	abc/αβ	No

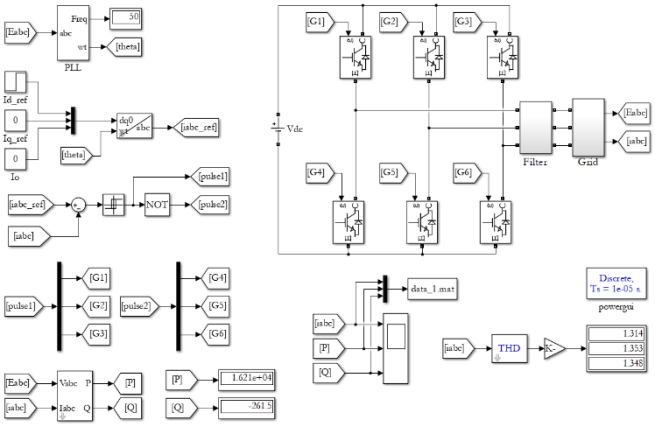

Figure 7: Simulink diagram of the hysteresis current control of the grid-connected three-phase inverter.

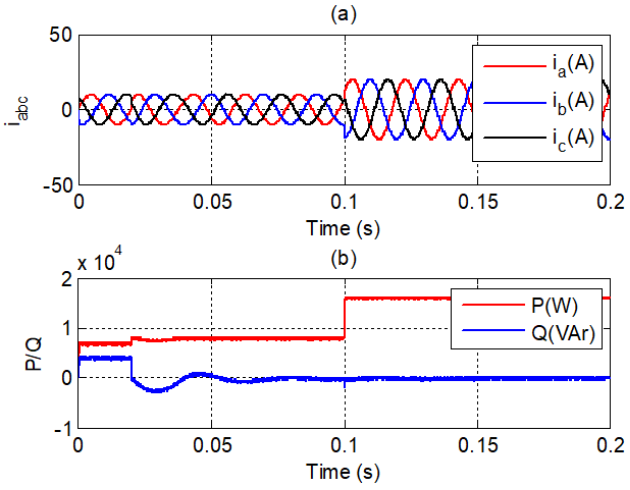

Figure 8: Hysteresis current control of the grid-connected three-phase inverter: (a) current waveforms and (b) grid-injected active and reactive power.

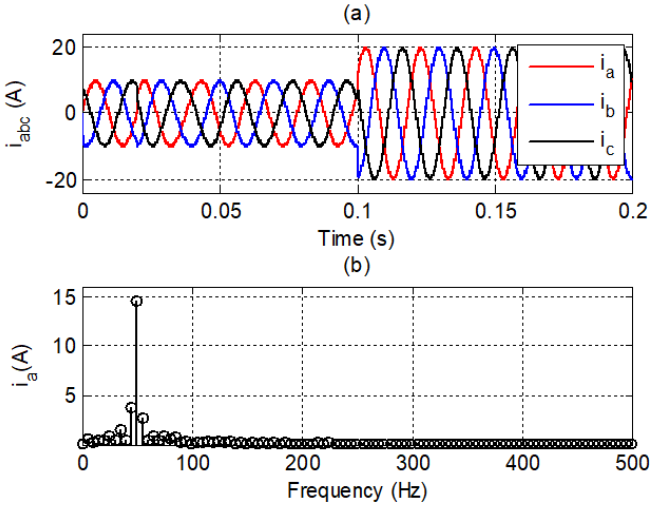

Figure 9: Hysteresis current control of the grid-connected three-phase inverter: (a) current waveforms and (b) FFT of the current waveform.

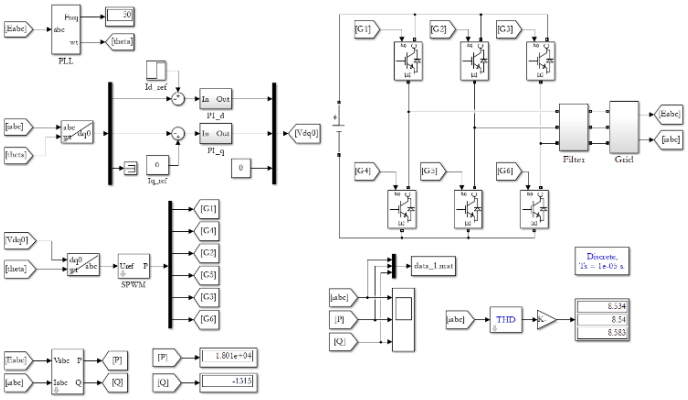

Figure 10: Simulink diagram of the SPWM current control of the grid-connected three-phase inverter.

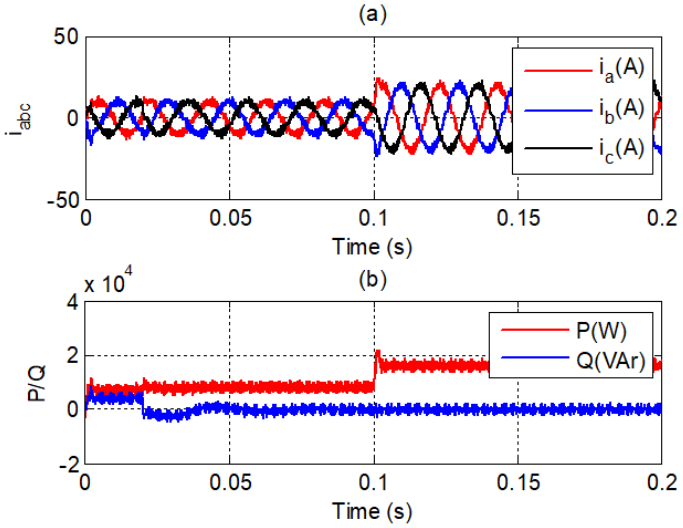

Figure 11: SPWM current control of the grid-connected three-phase inverter: (a) current waveforms and (b) grid-injected active and reactive power.

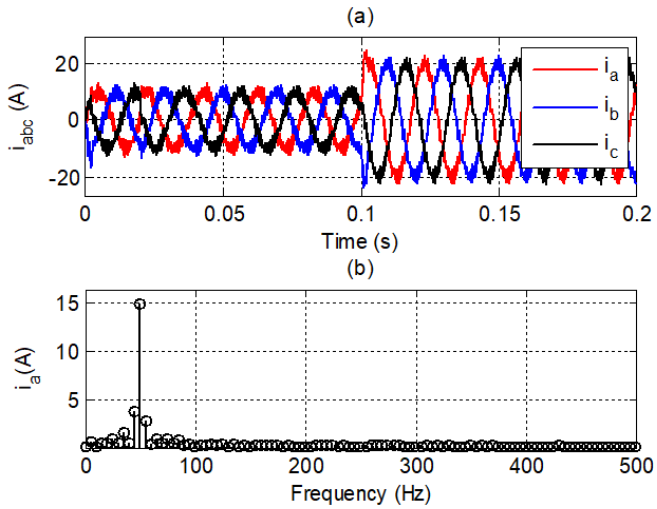

Figure 12: SPWM current control of the grid-connected three-phase inverter: (a) current waveforms and (b) FFT of the current waveform.

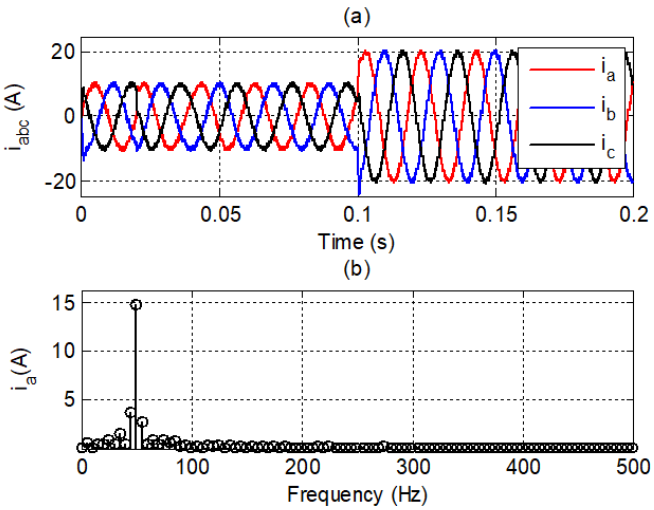

Figure 15: SVPWM current control of the grid-connected three-phase inverter: (a) current waveforms and (b) FFT of the current waveform.

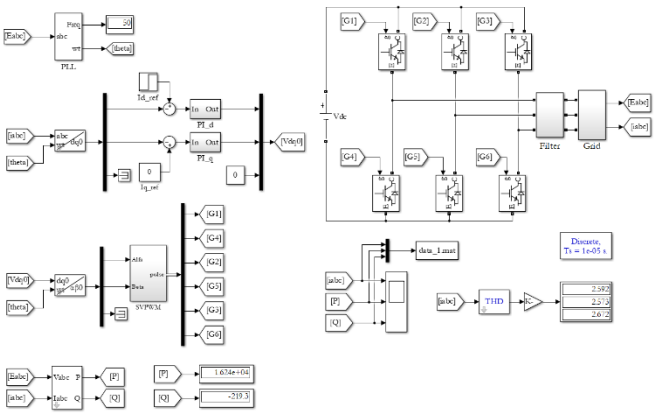

Figure 13: Simulink diagram of the SVPWM current control of the grid-connected three-phase inverter.

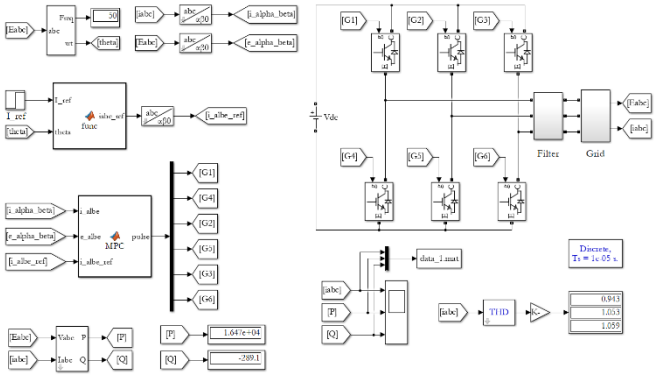

Figure 16: Simulink diagram of the predictive direct current control of the grid-connected three-phase inverter.

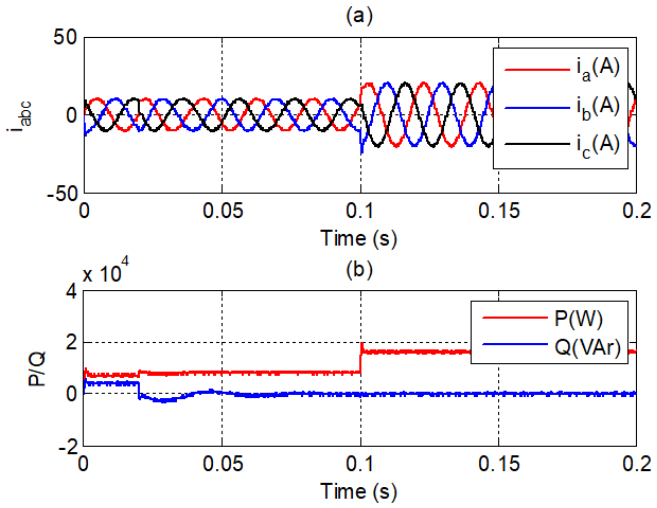

Figure 14: SVPWM current control of the grid-connected three-phase inverter: (a) current waveforms and (b) grid-injected active and reactive power.

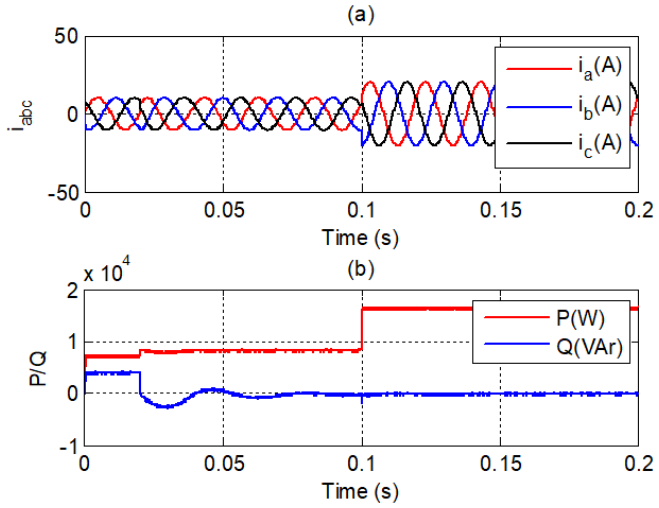

Figure 17: Predictive direct current control of the grid-connected three-phase inverter: (a) current waveforms and (b) grid-injected active and reactive power.

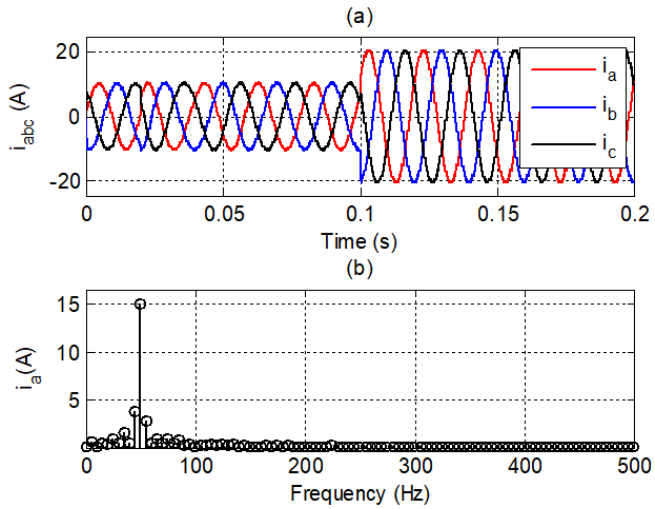

Figure 18: Predictive direct current control of the grid-connected three-phase inverter: (a) current waveforms and (b) FFT of the current waveform.

6.2. Predictive Direct Power Control of Grid-Connected Three-Phase Inverters

The principle of the predictive direct power control of the grid-connected three-phase is shown in Figure 19. In this case, the reference active power is firstly set to be 8(kW) and 20(kW) at the time of 0.1 seconds. The reference reactive power is assumed to be zero.

Table 5 is the MATLAB script of the predictive direct power control algorithm. The grid-injected active and reactive power can be optimally obtained as shown in Figure 20. The FFT of the current is depicted in Figure 21.

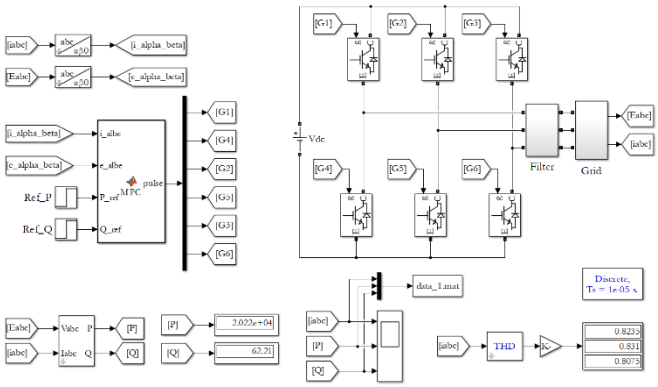

Figure 19: Simulink diagram of the predictive direct power control of the grid-connected PV three-phase inverter.

Table 5: The MATLAB script of predictive direct power control algorithm.

```
function pulse = MPC(i_albe, e_albe, P_ref, Q_ref)
R = 1;
L = 0.01;
Ts = 1e-5;
Vdc = 800;
i_alpha = i_albe(1);
i_beta = i_albe(2);
e_alpha = e_albe(1);
e_beta = e_albe(2);
Sa_opt = 0;
Sb_opt = 0;
Sc_opt = 0;
g_opt = inf;
for (Sa = 0:1)
   for (Sb = 0:1)
      for (Sc = 0:1)
         u_alpha = Vdc * (2 * Sa - Sb - Sc) / 3;
         u_beta = (2 / 3) * Vdc * ((sqrt(3)/2) * Sb - ((sqrt(3)/2)) * Sc);
         i_alpha1 = (Ts/(R*Ts + L))*(u_alpha-e_alpha) + ...
                    (L/(R*Ts + L)) * i_alpha;
         i_beta1 = (Ts/(R*Ts + L))*(u_beta-e_beta) + ...
                   (L/(R*Ts + L)) * i_beta;
         Pin1 = 3/2*(e_alpha*i_alpha1 + e_beta*i_beta1);
         Qin1 = 3/2*(e_beta*i_alpha1 - e_alpha*i_beta1);
         g = abs(Q_ref-Qin1) + abs(P_ref-Pin1);
         if (g < g_opt)
         Sa_opt = Sa;
         Sb_opt = Sb;
         Sc_opt = Sc;
         g_opt = g;
         end
      end
   end
end
Sa = Sa_opt;
Sb = Sb_opt;
Sc = Sc_opt;
pulse = [Sa; not(Sa); Sb; not(Sb); Sc; not(Sc)];
```

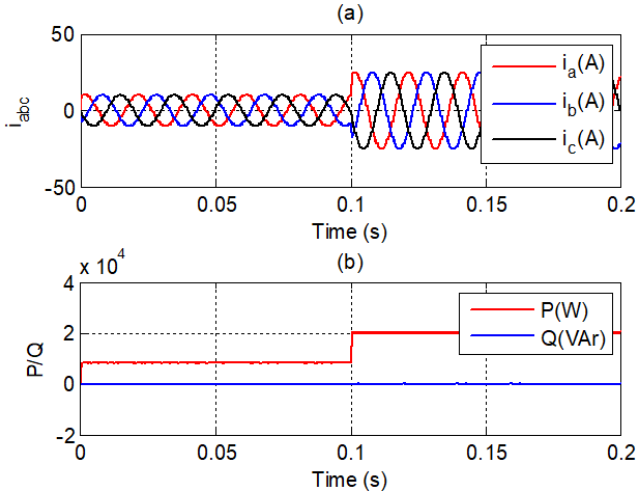

Figure 20: Predictive direct power control of the grid-connected PV three-phase inverter: (a) current waveforms and (b) grid-injected active and reactive power.

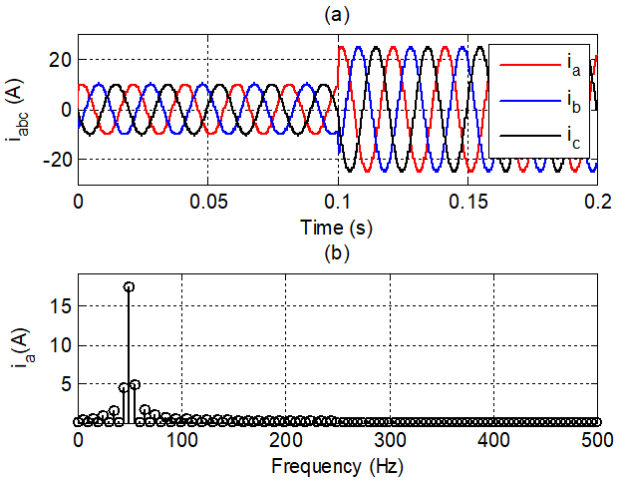

Figure 21: Predictive direct power control of the grid-connected PV three-phase inverter: (a) current waveforms and (b) FFT of the current waveform.

6.3. Predictive Direct Power Control of Grid-Connected PV Three-Phase Inverters

Table 6 is the parameters of the commercial PV panel used for simulation. Figure 22 is the Simulink diagram of the predictive direct power control of the grid-connected PV three-

phase inverter. Figure 23(a) is the current waveforms and Figure 23(b) is the grid-injected active and null reactive power with very small oscillations. Figure 24(a) is the current waveforms and Figure 24(b) is the FFT of the current.

Table 6: Parameters of the commercial PV panel used for simulation.

Parameters	Values
Nominal short-circuit voltage	Iscn = 5.11 (A)
Nominal array open-circuit voltage	Vocn = 29.80 (V)
Panel current at maximum power point	Ipvn = 4.74 (A)
Panel voltage at maximum power point	Vmp = 25.15 (V)
Panel maximum output peak power	Pmax_e = 120 (W)
Voltage/temperature coefficient	Kv = -0.38 (V/K)
Current/temperature coefficient	Ki = 0.04 (A/K)
Series resistance	Rs = 0.1683 (Ω)
Parallel resistance	Rp = 211.5173 (Ω)
Nominal irradiance	Gn = 1000 (W/m^2)
Nominal operating temperature	Tn = 25 + 273.15 (K)
Boltzmann constant	k = 1.3806503e-23 (J/K)
Electron charge	q = 1.60217646e-19 (C)
Ideal diode factor	a = 1

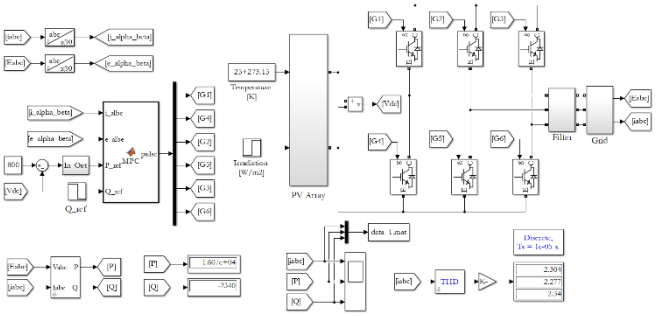

Figure 22: Simulink diagram of the predictive direct power control of grid-connected PV three-phase inverter.

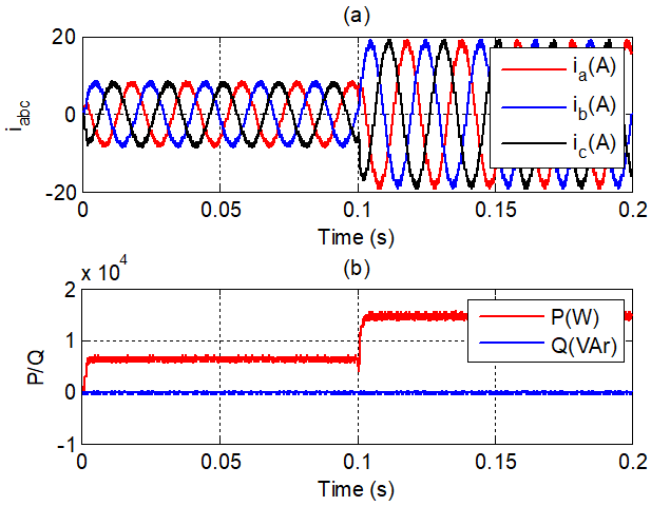

Figure 23: Predictive direct power control of grid-connected PV three-phase inverter : (a) current waveforms and (b) grid-injected active and reactive power.

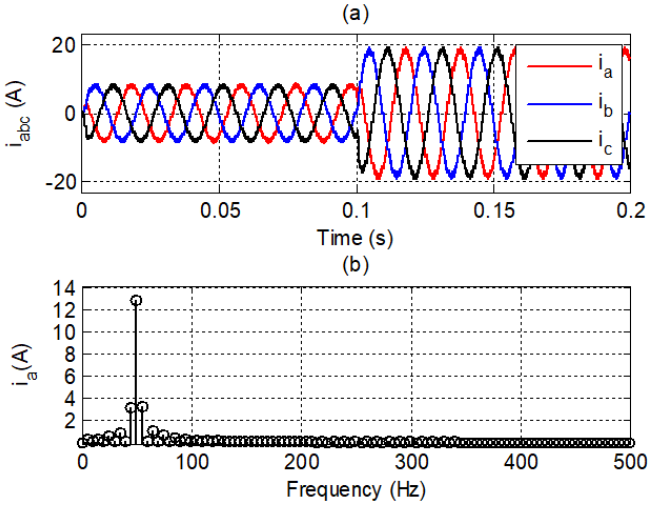

Figure 24: Predictive direct power control of the grid-connected PV three-phase inverter: (a) current waveforms and (b) FFT of the current waveform.

7. Conclusion

This research successfully demonstrates the useful use of MPC for directly controlling the active and reactive power generated by a grid-connected PV system. The proposed control algorithm operates in discrete-time and does not require any modulator or PLL to properly drive the inverter switches. In addition, the control architecture proposed requires no external control loops. Simulation results indicate a good tracking of the dynamic power reference formed by the maximum power tracking of solar energy. A good transient performance can be achieved without the significant oscillations of the grid-injected active and reactive power.

References

[1] Yang Chen, Keyue Smedley, *Three-Phase Boost-Type Grid-Connected Inverter*, IEEE Transactions on Power Electronics, vol: 23, no: 5, Sept. 2008, pp. 2301 - 2309, Sept. 2008

[2] Truong Quoc Thuong, Ngo Van Quyen, Nguyen Thanh Son, Nguyen The Cong, *Implementation of the controllers for maximum power point tracking of solar panel using LabVIEW*, Journal of Science and Technology, Vietnam, September 2014.

[3] Nguyen Thanh Son, Pham Hung Phi, Nguyen The Cong, Le Anh Tuan, Pham Van Tuan, *Model predictive current control of grid-connected three-phase inverter for PV systems*, Journal of Science and Technology, Vietnam, vol: 57, no: 2, , pp. 15 -19, April 2021.

[4] M. A. Mahmud, H. R. Pota, M. J. Hossain, *Nonlinear Current Control Scheme for a Single-Phase Grid-Connected Photovoltaic System*, IEEE Transactions on Sustainable Energy, vol: 5, no: 1, pp. 218 - 227, Jan. 2014.

[5] Jiabing Hu, Lei Shang, Yikang He, Z. Q. Zhu, *Direct Active and Reactive Power Regulation of Grid-Connected DC/AC Converters Using Sliding Mode Control Approach*, IEEE Transactions on Power Electronics, vol: 26, no: 1, pp. 210 - 222, Jan. 2011.

[6] Shuhui Li, Michael Fairbank, Cameron Johnson, Donald C. Wunsch, Eduardo Alonso, Julio L. Proao, *Artificial Neural Networks for Control of a Grid-Connected Rectifier/Inverter Under Disturbance, Dynamic and Power Converter Switching Conditions*, IEEE Transactions on Neural Networks and Learning Systems, vol: 25, no: 4, pp. 738 - 750, April 2014.

[7] M. A. Hannan, Zamre Abd. Ghani, Azah Mohamed, M. Nasir Uddin, *Real-Time Testing of a Fuzzy-Logic-Controller-Based Grid-Connected Photovoltaic Inverter System*, IEEE Transactions on Industry Applications, vol: 51, no: 6, pp. 4775 - 4784, Nov -Dec. 2015.

[8] S. Kouro, P. Cortés, R. Vargas, U. Ammann, J. Rodríguez, *Model Predictive Control - A Simple and Powerful Method to Control Power Converters*. IEEE Transactions on Industrial Electronics, vol. 56, no. 6, pp. 1826 - 1838, Jun 2009.

[9] Patricio Cortés, Gabriel Ortiz, Juan I. Yuz, José Rodríguez, Sergio Vazquez, and Leopoldo G. Franquelo, *Model Predictive Control of an Inverter With Output LC Filter for UPS Applications*, IEEE Transactions on Industrial Electronics, vol. 56, no. 6, pp. 1875-1883, June 2009.